JACS
JOURNAL OF THE AMERICAN CHEMICAL SOCIETY

Article

pubs.acs.org/JACS

Combined CO_2-philicity and Ordered Mesoporosity for Highly Selective CO_2 Capture at High Temperatures

Ji Hoon Lee, Hyeon Jeong Lee, Soo Yeon Lim, Byung Gon Kim, and Jang Wook Choi*

Graduate School of Energy, Environment, Water, and Sustainability (EEWS), Saudi Aramco-KAIST CO_2 Management Center, and Center for Nature-inspired Technology (CNiT) in KAIST Institute NanoCentury, Korea Advanced Institute of Science and Technology (KAIST), 291 Daehakro, Yuseong-gu, Daejeon 305-701, Republic of Korea

Supporting Information

ABSTRACT: Various dry sorbents have been lately introduced as promising media to capture carbon dioxide (CO_2). However, it is still desirable to further improve their performance in diverse aspects, and high temperature selectivity of CO_2 over other gases is clearly one of them. Here, we report a co-assembly approach to turn nonporous melamine resin to a highly ordered mesoporous polymeric network (space group: $Im\bar{3}m$) containing high nitrogen content (~18 at%). This mesoporous network shows anomalously increasing CO_2/N_2 selectivity with temperature rise, with the selectivity at 323 K reaching 117 (Henry method). This selectivity behavior is attributed to a combined effect of the high nitrogen content allowing for high binding affinity with CO_2 and well-defined mesopores (2.5−2.9 nm) accelerating release of N_2 with temperature rise. The given orthogonal approach suggests a new direction in designing dry sorbents with excellent selectivities at high temperatures.

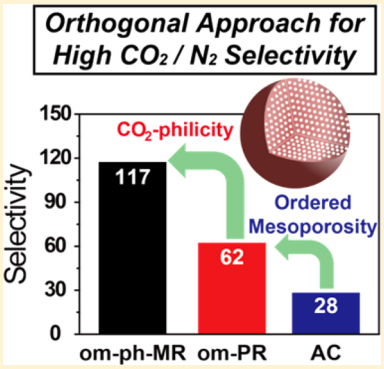

1. INTRODUCTION

The ever-increasing carbon dioxide (CO_2) emission from burning fossil fuels has been considered the main origin of various recent environment and energy issues.[1,2] In an effort to overcome this grand challenge, a global integrated measure, namely CO_2 capture and sequestration (CCS), has been launched with drawing a great deal of attention and regarded as one of the viable solutions.[3−5] In the area of CO_2 capture, various kinds of dry sorbents[5−10] have been lately investigated as alternatives to the current commercial technology using aqueous ethanolic amines[3,4] because the commercial technology suffers from intrinsic drawbacks represented by high energy penalty for regeneration and severe corrosion. In spite of the considerable progress so far, it is desirable to further improve performance in key aspects,[7] such as total CO_2 uptake, CO_2 selectivity over other gases especially nitrogen (N_2), and uptake retention upon temperature rise.

While the performance of dry sorbents is highly dependent on their various material parameters including specific surface area,[11,12] functional group,[13−18] and element,[19−22] it was recently revealed[18−20,22] that high nitrogen (N)-content can result in high uptake and selectivity simultaneously. In particular, the high selectivity was recently explained by a new concept, so-called N_2-phobicity.[18] In terms of taking advantage of high N-content, melamine (2,4,6-triamino-1,3,5-triazine) is one of the most ideal moieties for the sorbent building block because of its rich nitrogen content reaching twice as large as carbon. Melamine has additional advantages of low cost and long industrial history.[23−25] Despite the high N-content, the widely adopted form of melamine, melamine resin (MR), synthesized via continuous condensation reaction[26−31] between melamine and formaldehyde is not appropriate for CO_2 capture because its morphology is nonporous and its specific surface area is therefore pretty low (<2 m^2/g in this study) (see Figures S1−S2).

The synthesis of porous MR is inherently nontrivial.[26,29−31] The aforementioned condensation process is very reactive and propagates rapidly in random directions, eliminating the capability for morphology control. Other reaction schemes that activate melamine toward a polymeric network while incorporating a reagent serving as bridges for a porous framework are hardly available. The formation of MR is not also compatible with self-assembly with diverse surfactants because MR does not have any hydrogen bonding sites with surfactants. In the current study, we overcome this difficulty by developing a copolymer approach engaging phenolic resin (PR) units. The PR units are allowed to form hydrogen bonding[32−35] with a well-known surfactant, Pluronic F127 (a block copolymer, poly(ethylene oxide)$_{106}$-poly(propylene oxide)$_{70}$-poly(ethylene oxide)$_{106}$), to produce a highly ordered mesoporous copolymer network with a high nitrogen content (~18 at%). The high N-content originating from the triazine units of melamine facilitates strong CO_2 binding affinity, enabling "CO_2-philicity", while well-defined pores in a mesoscopic dimension (~2.9 nm) disrupt N_2 adsorption especially at high temperatures due to weakened interaction with pore walls. This orthogonal approach to the two different gases results in excellent CO_2-to-N_2 selectivities and an unusual selectivity increase over temperature rise, implying that mesopores are useful in enhancing the selectivity. Also, the

Received: April 6, 2015
Published: May 22, 2015

DOI: 10.1021/jacs.5b03579
J. Am. Chem. Soc. 2015, 137, 7210−7216

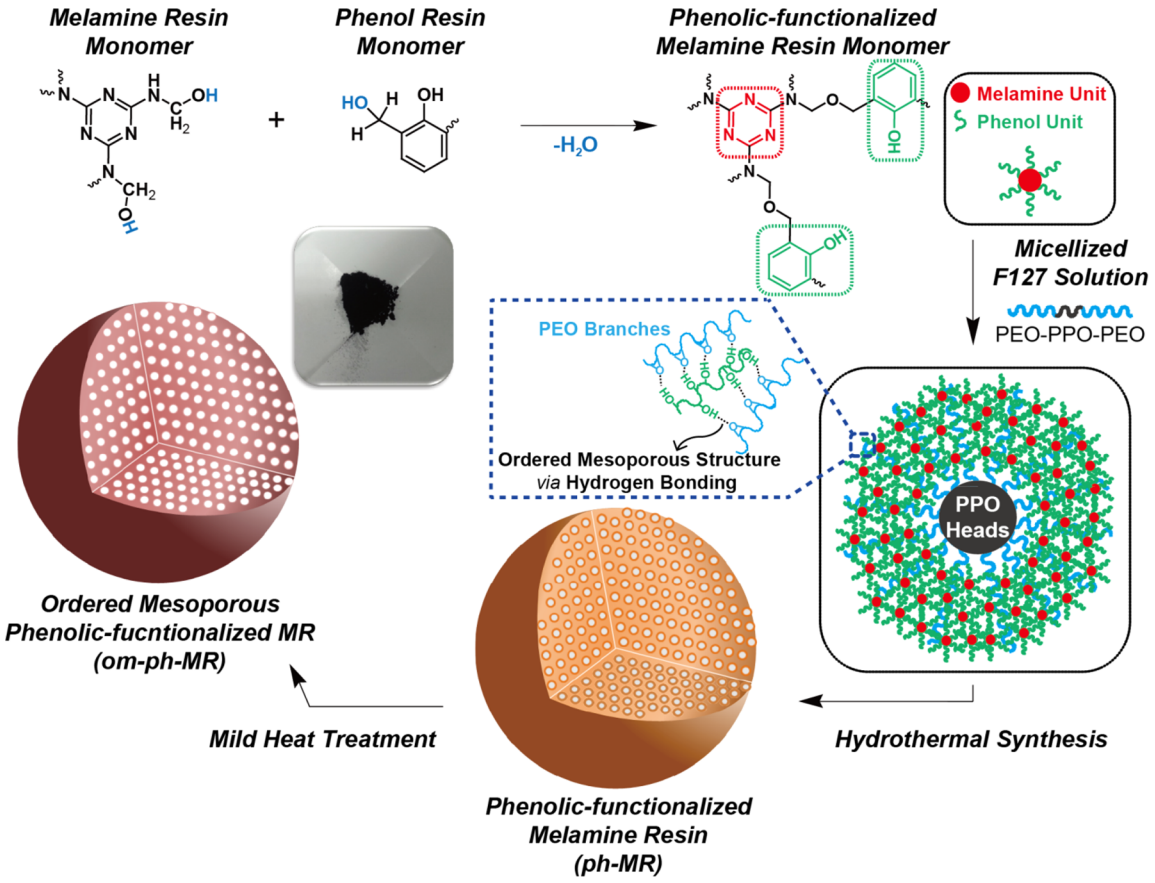

Figure 1. Schematic representation showing the synthetic route of ordered mesoporous phenolic-functionalized melamine resin (om-ph-MR).

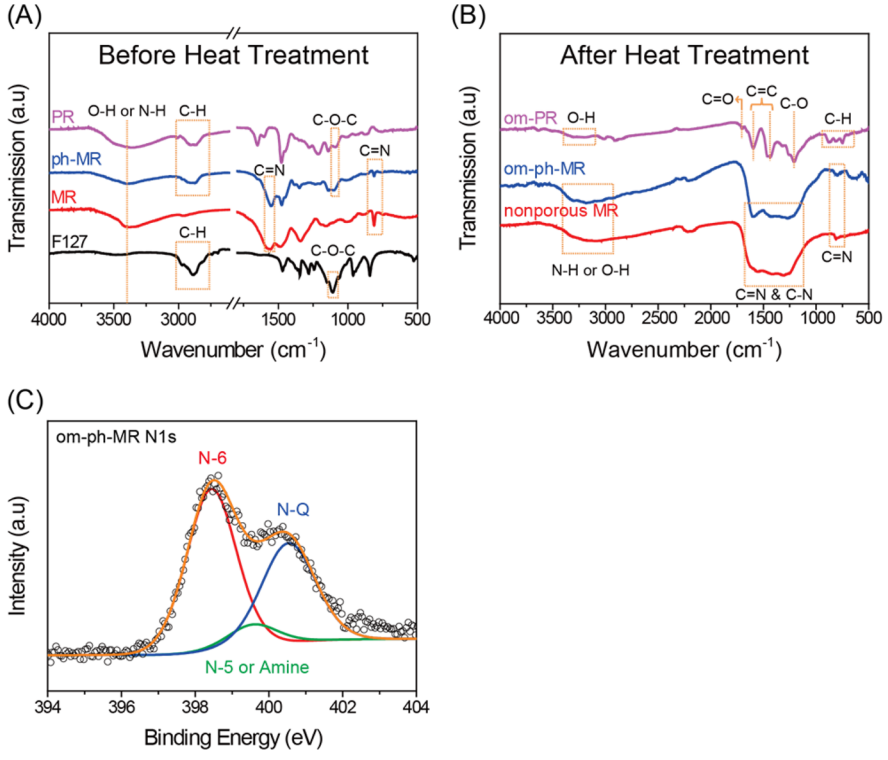

Figure 2. Spectroscopy analyses of om-ph-MR. FT-IR spectra (A) before and (B) after a mild heat treatment. (C) XPS spectrum in the N 1s branch.

present study with highly organized mesopores could offer a clue to resolve the recent inconsistent selectivities of the porous polymers with the same nitrogen-containing functional groups.[16−18]

DOI: 10.1021/jacs.5b03579
J. Am. Chem. Soc. 2015, 137, 7210−7216

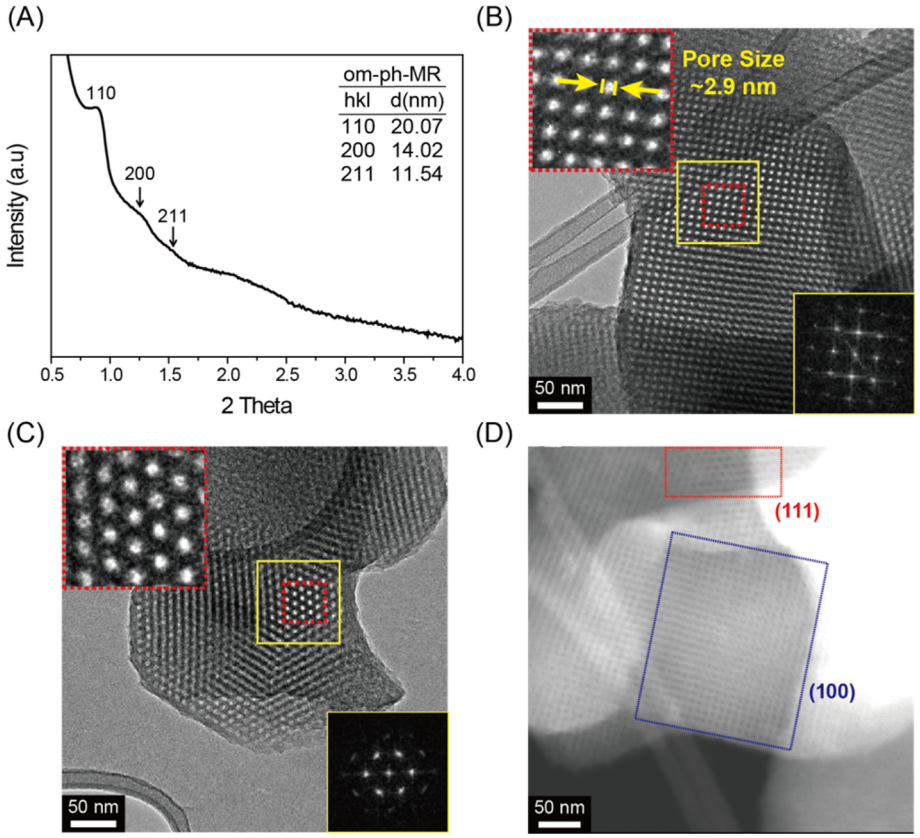

Figure 3. (A) Powder SAXS pattern for om-ph-MR. HRTEM images of om-ph-MR viewed in the (B) [100] and (C) [111] zone axes. Bottom-right insets are FT patterns attained from the yellow boxes. Top-left insets are zoomed-in images from the red boxes. (D) Scanning TEM image of om-ph-MR showing both the (100) and (111) planes.

2. RESULTS AND DISCUSSION

Once MR monomer is reacted with PR monomer via condensation, phenolic-functionalized melamine resin (ph-MR) monomer can be generated (see Figure 1). The ph-MR monomer can form hydrogen bonding with F127 through interactions between its phenol groups and the ethylene oxide (EO) groups in the PEO branches of F127.[32−35] A subsequent hydrothermal process leads to an assembly with an ordered mesostructure, which is then converted to final ordered mesoporous ph-MR (denoted as om-ph-MR) after removing F127 by a mild heat treatment at 400 °C (see thermogravimetric analysis (TGA) data in Figure S3).[34,35] Detailed experimental procedure is described in the Experimental Section in Supporting Information.

Fourier-transform infrared (FT-IR) spectra before the heat treatment (Figure 2A) confirm the assembly of ph-MR with F127, as the spectrum of ph-MR showed peaks at ∼2870 and ∼1117 cm^{-1} corresponding to the C−H stretching vibration of methylene group and the C−O stretching vibration of the ether group in F127,[36,37] respectively, in contrast with bare MR. The given signals were also detected in the spectra of PR and F127. Hence, these FT-IR results are well aligned with the aforementioned hydrogen-bonding formation between ph-MR and F127. In addition, the peaks at 1580 and 800 cm^{-1} assigned to the C═N stretching vibration of triazine ring[31,38−40] were observed for ph-MR and MR, verifying that the melamine identity was preserved in ph-MR. Overall, the FT-IR results support our synthetic strategy that the triazine moiety in melamine can be built into a mesoscopic ordered structure by incorporation with the phenolic functional group in the PR monomer.

Even after the mild heat treatment, the FT-IR peak at 800 cm^{-1} reflective of C═N bonds was maintained to a large extent (Figure 2B). However, the peak at 1580 cm^{-1} became broadened in the range of 1200−1600 cm^{-1}, which suggests that some of the C−N and C═N conjugation was disrupted, and these bonds were present separately to some degree.[38−40] Also, the peaks corresponding to F127 disappeared, verifying the removal of F127. In contrast, the FT-IR spectrum of om-PR confirms that the phenol moiety kept[34,35,41] its main chemical identity: C═C (∼1600 cm^{-1}), C═O (∼1700 cm^{-1}), and C−O (∼1200 cm^{-1}). In addition, X-ray photoemission spectroscopy (XPS) profile in N 1s branch of om-ph-MR exhibited two major peaks at 398.5 and 400.8 eV corresponding to N-6 (pyridine-like) and N-Q (graphite-like) carbon−nitrogen bonding configurations, along with a minor peak at 399.4 eV corresponding to N-5 (pyrrole-like) or amine configurations (Figures 2C and S4).[27,28,42] The presence of the N-6 and N-Q configurations is in good agreement with the FT-IR data that revealed the existence of C−N and C═N. An elemental analysis indicates that om-ph-MR contains a high nitrogen content of 18.16 at% (Table S1), which would play a key role in increasing the selectivity of CO_2 over N_2 as will be discussed later.

To obtain information on the structural ordering of om-ph-MR, small-angle X-ray scattering (SAXS) analysis was performed (Figure 3A). The SAXS pattern exhibited well-resolved diffraction peaks corresponding to (110), (200), and (211) Bragg reflections, indicating that om-ph-MR holds a highly ordered mesostructure under the space group $Im\bar{3}m$. The observed

DOI: 10.1021/jacs.5b03579
J. Am. Chem. Soc. 2015, 137, 7210−7216

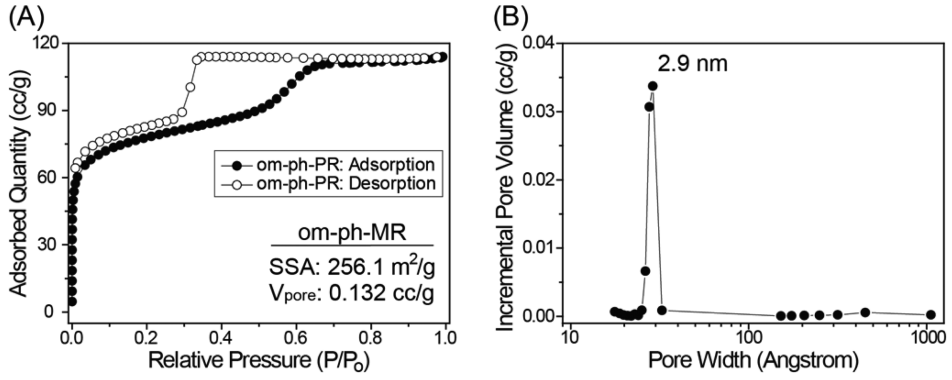

Figure 4. (A) Ar adsorption−desorption isotherms of om-ph-MR at 87 K. (B) Pore size distribution curve from the desorption branch using the BJH model.

Table 1. CO_2 and N_2 Uptakes, CO_2/N_2 Selectivities, and Isosteric Heats (Q_{st}) of om-ph-MR, om-PR, and AC

	CO_2 uptake[a]			N_2 uptake[a]			selectivity[b]			Q_{st}
T (K)	273	298	323	273	298	323	273	298	323	(kJ/mol)[c]
om-ph-MR	2.50	1.77	1.26	0.28	0.13	0.08	65	100	117	32.2
om-PR	1.91	1.24	0.79	0.19	0.10	0.05	54	50	62	31.4
AC	2.59	1.66	1.11	0.32	0.19	0.12	34	32	28	27.8

[a]Unit: mmol/g at 1 bar. [b]Obtained from initial slope of adsorption isotherm in linear low-pressure regime (0.0−0.1 bar). [c]Obtained from CO_2 isotherm data at 273 and 298 K using the Clausius−Clapeyron equation.

ordered structure is consistent with that of ordered mesoporous carbons with the same space group reported previously.[33,34,43,44] Scanning electron microscopy (SEM) images (Figure S5) of om-ph-MR showed a polyhedron shape, another indication of its ordered mesostructure.

To capture the ordered mesostructure in a more tangible manner, om-ph-MR was visualized by high-resolution transmission electron microscopy (HRTEM). When viewed along the [100] and [111] directions (Figure 3B,C, respectively), four-fold and three-fold symmetries of pores with high mesoscopic regularities were clearly observed, which is consistent with the body-centered cubic (bcc) symmetry belonging to the $Im\bar{3}m$ space group.[33,34,43,44] The corresponding Fourier transform patterns (insets of Figure 3B,C) also verify the observed geometries of the pore arrays. The HRTEM image (top left inset of Figure 3B) indicates that the pore size is approximately 2.9 nm. Moreover, the ordered mesoscopic structure was consistently observed by scanning TEM image (Figure 3D) that concurrently exhibited the two crystal orientations along the [111] and [100] zone axes.

Argon (Ar) adsorption/desorption isotherms provide a more quantitative set of information on the porosity of om-ph-MR (Figure 4A and Table 1). The isotherm with a sharp capillary condensation step at P/P_0 = ∼0.3 corresponds to type IV reflecting the dominant presence of mesopores. Brunauer−Emmet−Teller[45] specific surface area and pore volume turned out to be 256 m^2/g and 0.13 cc/g, respectively. The main pore size of ∼2.9 nm according to the Barrett−Joyner−Halenda (BJH)[46] method from the desorption branch (Figure 4B) is well matched with the bright core dimension of each pore in the TEM observation (inset of Figure 3B). If the adsorption branch is taken into account, the main pore size becomes ∼4.9 nm. These distinct pore sizes reflect bottle-like shape of the mesopores.[34] The series of analyses coherently imply that om-ph-MR holds a highly ordered mesoporous structure bearing N-6 and N-Q configurations as building components.

Next, CO_2 capture of om-ph-MR was investigated focusing on the effect of the N-containing units in the ordered porous framework. Two other porous materials, om-PR and activated carbon (AC), were also tested to further elucidate the role of the N-containing units and pore size. om-PR possesses the same $Im\bar{3}m$ space group (see SAXS pattern in Figure S6) as well as larger specific surface area and pore volume (385.9 m^2/g and 0.17 cc/g, Figures S7 and S8). Its main pore size is 2.5 nm according to the BJH method (Figure S7). om-PR consists mainly of benzene ring with oxygen-containing functional groups[34,41] and has 8.58 at% of oxygen according to XPS analysis (Figure S4). On the other hand, AC has been known to have slit-shaped micropores,[47] and the AC used in this study was synthesized to have similar specific surface area and pore volume (413.3 m^2/g and 0.15 cc/g, Figures S7 and S8) to those of the other samples to elucidate the pore size effect.

All of the samples showed reversible CO_2/N_2 isotherms at different temperatures (Figure 5), indicating physisorption-based uptake processes. om-ph-MR showed decent CO_2 uptakes of 110, 78, and 55 mg/g at 273, 298, and 323 K (Figure 5A−C), respectively, which are attributed to favorable quadrupole−dipole interaction[3,18,48−50] between polarizable CO_2 and the N-containing units. This favorable interaction is also reflected in higher isosteric heat of adsorption (Q_{st})[7,18,48,51] value (32.2 kJ/mol at the initial CO_2 loading) compared with those of the other two samples (Table 1 and Figure S9). Even with the favorable quadrupole−dipole interaction, the CO_2 binding of om-ph-MR is based mainly on physisorption, as Q_{st} is too small for chemisorption. The isotherm curves of om-ph-MR with no hysteresis are another evidence to support the physisorption. In our experiment, the same om-ph-MR sample was repeatedly measured at all the temperatures, and the consistent uptakes were confirmed, verifying that the porosity of om-ph-MR was not damaged during the measurements.

The enhanced interaction of om-ph-MR turns out more pronounced when the uptake is monitored as the temperature is

DOI: 10.1021/jacs.5b03579
J. Am. Chem. Soc. 2015, 137, 7210−7216

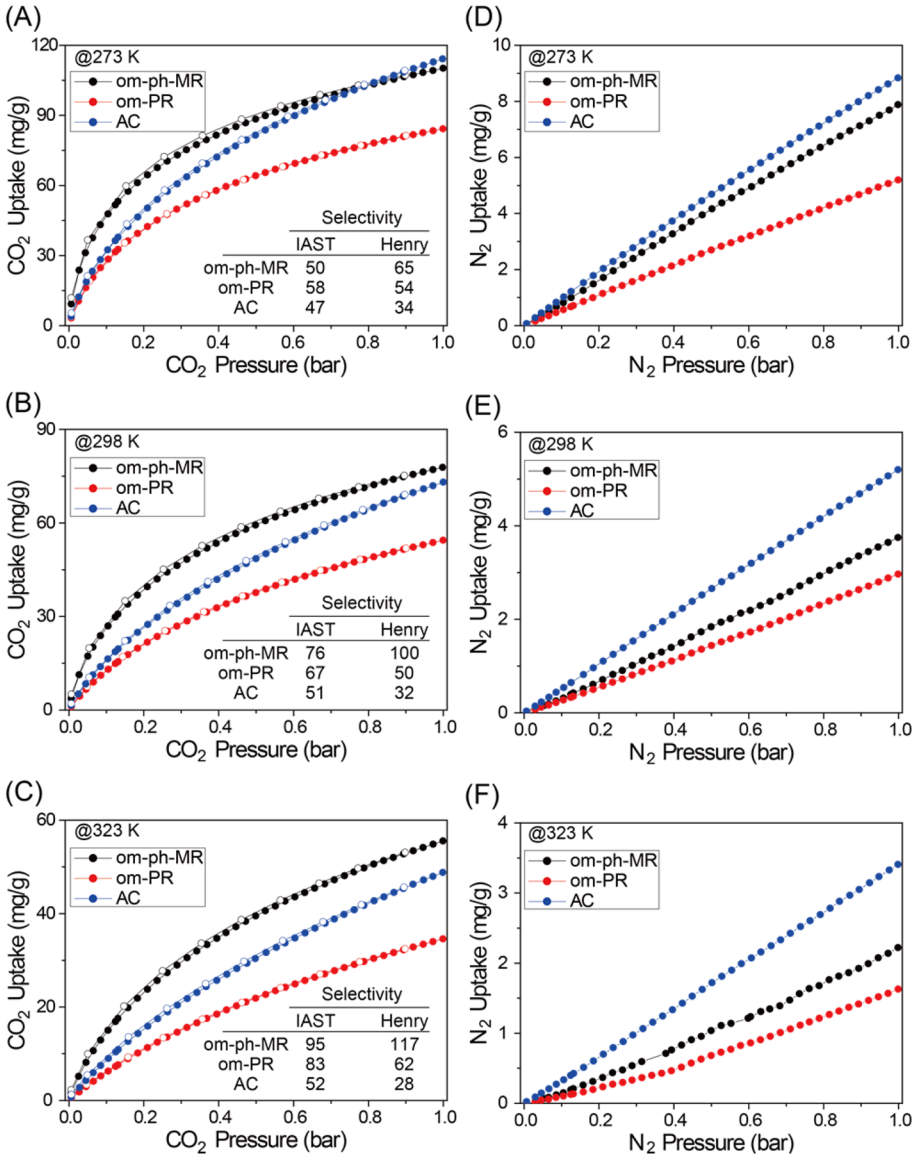

Figure 5. (A–C) CO_2 and (D–F) N_2 uptake isotherms for om-ph-MR (black), om-PR (red), and AC (blue) at 273, 298, and 323 K. Insets are the calculated CO_2/N_2 selectivities using both the IAST and the Henry's constants.

raised. When the temperature went up from 273 to 323 K at 1 bar, om-ph-MR retained 50.6% of the initial capacity, whereas om-PR and AC preserved only 41.1% and 42.8%, respectively (Table S2). At 0.15 bar, a realistic condition for actual flue gas, om-ph-MR also exhibited higher uptakes than those of the other two sorbents at all the temperatures tested, verifying the effective binding of the N-containing units with CO_2. The effective CO_2 binding is also reflected in the steep slopes of the CO_2 isotherms at low relative pressures. In particular, it is anticipated that a good portion of N-6 configuration (Figure 2C) in om-ph-MR plays a critical role in the favorable CO_2 binding by utilizing the excess electrons on the corresponding nitrogen, which is in good agreement with a recent computational study.[52]

For actual on-site application, besides high CO_2 uptake, high CO_2/N_2 selectivity especially at high temperatures is highly preferred.[2,3,7,18] om-ph-MR exhibited high selectivity as well as an unusual trend of selectivity increase upon the temperature rise (insets of Figure 5A–C): the Henry selectivity increased from 65 to 100 to 117 (Figure S10), as the temperature went from 273 to 298 to 323 K. The ideal adsorption solution theory (IAST)[53] selectivities (Figures S11–13 and Tables S3–S4) were consistent with the Henry's selectivities. Remarkably, the selectivities at 323 K, 95 (IAST), and 117 (Henry) are higher than those of most of other porous polymers[48,49,54–67] reported to date as summarized in Table S5. The anomalous selectivity increase with the temperature can be explained by both CO_2-philicity and mesoporosity and can be clarified further by a systematic comparison with the other two samples.

From the CO_2 and N_2 uptakes of the three samples (Figure 5 and Table 1) and their uptake retentions over the temperature range (Table S2), the critical role of CO_2-philicity and mesoporosity is unburied for om-ph-MR. In the CO_2 uptake retention viewpoint, for the same temperature rise from 273 to 323 K at 1 bar, om-ph-MR showed a better retention (50.6%) than those of the other two samples (41.1% for om-PR and 42.8% for AC), which can be once again explained by the CO_2 affinity of the N-containing units. In the absence of such binding capability, om-PR and AC exhibited similarly lower retentions. The higher quadrupole moment and polarizability of CO_2 than those of N_2 by 2.85 and 1.5 times,[3,18,68] respectively, are the

DOI: 10.1021/jacs.5b03579
J. Am. Chem. Soc. 2015, 137, 7210–7216

origin in having this CO_2-philic interaction in effect. By contrast, the behavior of N_2 uptake retention was opposite. At the same temperature increase and pressure, while om-ph-MR and om-PR showed similar retentions of 26.7% and 28.9%, respectively, AC exhibited a far higher retention of 38.6% (Table S2), implying that mesopores are better at releasing N_2 with the temperature rise.

Pore size is definitely critical for gas capture. In general, the capturing capability drops as the pore size increases due to the weakened interaction with gas molecules.[69] The superior N_2 retention of the AC over the temperature range can also be explained by its smaller pore sizes (<1.5 nm, Figure S7). In the case of om-ph-MR and om-PR, even under the same unfavorable situation from the larger pore sizes, CO_2 uptake retention of om-ph-MR over the temperature range is less interfered due to the aforementioned CO_2 binding affinity of the N-containing units. Hence, once again, the combined CO_2-philicity from the N-containing units and mesoporosity accelerating N_2 release with the temperature rise is the origin of the observed high selectivities of om-ph-MR at high temperatures. Control om-ph-MR samples heat treated at higher temperatures exhibited inferior selectivities (Figures S14 and S15), which are attributed to increased micropore portion and decreased N-content (Table S1). In the same line, it is anticipated that the recently reported inconsistent CO_2/N_2 selectivity behaviors of the same or very similar azo-linked porous polymers[16−18] might be due to the distinct portions of mesopores. In fact, in the case[18] that selectivity enhancement with temperature rise was observed, the particle diameter was 20−50 nm so the interparticle mesopores account for a good portion of its porosity as evidenced by its isotherms. More strictly speaking, the critical pore size that begins to lose CO_2 binding is below 1 nm[69] (although it would be material dependent) and is thus different from the conventional boundary (2 nm) between micropores and mesopores. In any case, the present investigation indicates that a large portion of pores bigger than the critical pore size in the presence of high N-content can facilitate anomalous selectivity increase over the temperature rise. According to *t*-plot method (Figure S16),[70] micropores of om-ph-MR occupy 32% of its pore volume. However, these micropores are unlikely to be the origin of the increased selectivity over the temperature rise since micropores would enhance the N_2 retention over the increased temperature. Another strong evidence is that most of N-containing polymers[16,17,48] consisting mainly of micropores also did not show such selectivity enhancement over the temperature rise.

3. CONCLUSION

In conclusion, we have reported a new synthesis that turns melamine resin mesoporous with a highly ordered pore arrangement. The current copolymer approach should be applicable to other similar resin moieties that cannot form hydrogen binding with most surfactants. In the CO_2 capturing perspective, the copresence of high N-content and mesoporosity handles CO_2 and N_2 in an orthogonal manner, giving rise to unusual high selectivities at high temperatures. Hence, the current study offers a useful design principle for superior selectivities of porous dry sorbents at high temperatures, namely combined mesopores and functional groups with high binding affinity with CO_2.

■ ASSOCIATED CONTENT

Supporting Information

Information regarding experimental section, additional CO_2/N_2 isotherm curves, TGA data, XPS spectra, high-resolution SEM images, SAXS patterns, isosteric heats of adsorption, IAST/Henry selectivity graphs, *t*-plot graphs, elemental content table, and selectivity comparison table. The Supporting Information is available free of charge on the ACS Publications website at DOI: 10.1021/jacs.5b03579.

■ AUTHOR INFORMATION

Corresponding Author

*jangwookchoi@kaist.ac.kr

Notes

The authors declare no competing financial interest.

■ ACKNOWLEDGMENTS

We acknowledge financial support by the Saudi Aramco-KAIST CO_2 Management Center and the National Research Foundation of Korea (NRF) grant funded by the Korea government (MEST) (NRF-2014R1A4A1003712).

■ REFERENCES

(1) Morello, L. *Nature* **2014**, *513*, 289−289.
(2) House, K. Z.; Baclig, A. C.; Ranjan, M.; van Nierop, E. A.; Wilcox, J.; Herzog, H. J. *Proc. Natl. Acad. Sci. U.S.A.* **2011**, *108*, 20428−20433.
(3) D'Alessandro, D. M.; Smit, B.; Long, J. R. *Angew. Chem., Int. Ed.* **2010**, *49*, 6058−6082.
(4) Rochelle, G. T. *Science* **2009**, *325*, 1652−1654.
(5) Sumida, K.; Rogow, D. L.; Mason, J. A.; McDonald, T. M.; Bloch, E. D.; Herm, Z. R.; Bae, T. H.; Long, J. R. *Chem. Rev.* **2012**, *112*, 724−781.
(6) Li, G.; Xiao, P.; Webley, P.; Zhang, J.; Singh, R.; Marshall, M. *Adsorption* **2008**, *14*, 415−422.
(7) Samanta, A.; Zhao, A.; Shimizu, G. K. H.; Sarkar, P.; Gupta, R. *Ind. Eng. Chem. Res.* **2012**, *51*, 1438−1463.
(8) Sircar, S.; Golden, T. C.; Rao, M. B. *Carbon* **1996**, *34*, 1−12.
(9) Yazaydin, A. O.; Snurr, R. Q.; Park, T.-H.; Koh, K.; Liu, J.; LeVan, M. D.; Benin, A. I.; Jakubczak, P.; Lanuza, M.; Galloway, D. B.; Low, J. J.; Willis, R. R. *J. Am. Chem. Soc.* **2009**, *131*, 18198−18199.
(10) Yue, M. B.; Chun, Y.; Cao, Y.; Dong, X.; Zhu, J. H. *Adv. Funct. Mater.* **2006**, *16*, 1717−1722.
(11) Ma, X. Y.; Li, Y.; Cao, M. H.; Hu, C. W. *J. Mater. Chem. A* **2014**, *2*, 4819−4826.
(12) Wickramaratne, N. P.; Jaroniec, M. *ACS Appl. Mater. Interfaces* **2013**, *5*, 1849−1855.
(13) Dawson, R.; Adams, D. J.; Cooper, A. I. *Chem. Sci.* **2011**, *2*, 1173−1177.
(14) Torrisi, A.; Mellot-Draznieks, C.; Bell, R. G. *J. Chem. Phys.* **2009**, *130*, 194703.
(15) Torrisi, A.; Mellot-Draznieks, C.; Bell, R. G. *J. Chem. Phys.* **2010**, *132*, 044705.
(16) Arab, P.; Rabbani, M. G.; Sekizkardes, A. K.; Islamoglu, T.; El-Kaderi, H. M. *Chem. Mater.* **2014**, *26*, 1385−1392.
(17) Lu, J.; Zhang, J. *J. Mater. Chem. A* **2014**, *2*, 13831−13834.
(18) Patel, H. A.; Je, S. H.; Park, J.; Chen, D. P.; Jung, Y.; Yavuz, C. T.; Coskun, A. *Nat. Commun.* **2013**, *4*, 1357.
(19) Chandra, V.; Yu, S. U.; Kim, S. H.; Yoon, Y. S.; Kim, D. Y.; Kwon, A. H.; Meyyappan, M.; Kim, K. S. *Chem. Commun.* **2012**, *48*, 735−737.
(20) Nandi, M.; Okada, K.; Dutta, A.; Bhaumik, A.; Maruyama, J.; Derks, D.; Uyama, H. *Chem. Commun.* **2012**, *48*, 10283−10285.
(21) Seema, H.; Kemp, K. C.; Le, N. H.; Park, S.-W.; Chandra, V.; Lee, J. W.; Kim, K. S. *Carbon* **2014**, *66*, 320−326.
(22) Xing, W.; Liu, C.; Zhou, Z.; Zhang, L.; Zhou, J.; Zhuo, S.; Yan, Z.; Gao, H.; Wang, G.; Qiao, S. Z. *Energy Environ. Sci.* **2012**, *5*, 7323−7327.
(23) Lund, K. H.; Petersen, J. H. *Food Addit. Contam.* **2006**, *23*, 948−955.
(24) Hong, K.; Park, S. *Mater. Chem. Phys.* **1999**, *58*, 128−131.
(25) Chien, C.-Y.; Wu, C.-F.; Liu, C.-C.; Chen, B.-H.; Huang, S.-P.; Chou, Y.-H.; Chang, A.-W.; Lee, H.-H.; Pan, C.-H.; Wu, W.-J.; Shen, J.-T.; Chang, M.-Y.; Huang, C.-H.; Shiea, J.; Hsieh, T.-J.; Wu, M.-T. *J. Hazard. Mater.* **2011**, *188*, 350−356.

DOI: 10.1021/jacs.5b03579
J. Am. Chem. Soc. 2015, 137, 7210−7216

(26) Kim, S. Y.; Suh, W. H.; Choi, J. H.; Yi, Y. S.; Lee, S. K.; Stucky, G. D.; Kang, J. K. *J. Mater. Chem. A* **2014**, *2*, 2227−2232.
(27) Jeong, H. M.; Lee, S. Y.; Shin, W. H.; Kwon, J. H.; Shakoor, A.; Hwang, T. H.; Kim, S. Y.; Kong, B.-S.; Seo, J.-S.; Lee, Y. M.; Kang, J. K.; Choi, J. W. *RSC Adv.* **2012**, *2*, 4311−4317.
(28) Lee, J. H.; Park, N.; Kim, B. G.; Jung, D. S.; Im, K.; Hur, J.; Choi, J. W. *ACS Nano* **2013**, *7*, 9366−9374.
(29) Pevida, C.; Drage, T. C.; Snape, C. E. *Carbon* **2008**, *46*, 1464−1474.
(30) Wilke, A.; Weber, J. *J. Mater. Chem.* **2011**, *21*, 5226−5229.
(31) Ma, F.; Zhao, H.; Sun, L.; Li, Q.; Huo, L.; Xia, T.; Gao, S.; Pang, G.; Shi, Z.; Feng, S. *J. Mater. Chem.* **2012**, *22*, 13464−13468.
(32) Liang, C. D.; Dai, S. *J. Am. Chem. Soc.* **2006**, *128*, 5316−5317.
(33) Fang, Y.; Gu, D.; Zou, Y.; Wu, Z.; Li, F.; Che, R.; Deng, Y.; Tu, B.; Zhao, D. *Angew. Chem., Int. Ed.* **2010**, *49*, 7987−7991.
(34) Meng, Y.; Gu, D.; Zhang, F.; Shi, Y.; Cheng, L.; Feng, D.; Wu, Z.; Chen, Z.; Wan, Y.; Stein, A.; Zhao, D. *Chem. Mater.* **2006**, *18*, 4447−4464.
(35) Zhang, F. Q.; Meng, Y.; Gu, D.; Yan, Y.; Yu, C. Z.; Tu, B.; Zhao, D. Y. *J. Am. Chem. Soc.* **2005**, *127*, 13508−13509.
(36) Wang, Y.; Su, Y.; Sun, Q.; Ma, X.; Ma, X.; Jiang, Z. *J. Membr. Sci.* **2006**, *282*, 44−51.
(37) Lv, C.; Su, Y.; Wang, Y.; Ma, X.; Sun, Q.; Jiang, Z. *J. Membr. Sci.* **2007**, *294*, 68−74.
(38) Zhao, Y.; Liu, Z.; Chu, W.; Song, L.; Zhang, Z.; Yu, D.; Tian, Y.; Xie, S.; Sun, L. *Adv. Mater.* **2008**, *20*, 1777−1781.
(39) Holst, J. R.; Gillan, E. G. *J. Am. Chem. Soc.* **2008**, *130*, 7373−7379.
(40) Zhang, Y.; Thomas, A.; Antonietti, M.; Wang, X. *J. Am. Chem. Soc.* **2009**, *131*, 50−51.
(41) Holopainen, T.; Alvila, L.; Rainio, J.; Pakkanen, T. T. *J. Appl. Polym. Sci.* **1998**, *69*, 2175−2185.
(42) Jeong, H. M.; Lee, J. W.; Shin, W. H.; Choi, Y. J.; Shin, H. J.; Kang, J. K.; Choi, J. W. *Nano Lett.* **2011**, *11*, 2472−2477.
(43) Hao, G.-P.; Li, W.-C.; Qian, D.; Wang, G.-H.; Zhang, W.-P.; Zhang, T.; Wang, A.-Q.; Schueth, F.; Bongard, H.-J.; Lu, A.-H. *J. Am. Chem. Soc.* **2011**, *133*, 11378−11388.
(44) Lee, J.; Kim, J.; Hyeon, T. *Adv. Mater.* **2006**, *18*, 2073−2094.
(45) Brunauer, S.; Emmett, P. H.; Teller, E. *J. Am. Chem. Soc.* **1938**, *60*, 309−319.
(46) Barret, E. P.; Joyner, L. G.; Halenda, P. P. *J. Am. Chem. Soc.* **1951**, *73*, 373−380.
(47) Guo, J.; Morris, J. R.; Ihm, Y.; Contescu, C. I.; Gallego, N. C.; Duscher, G.; Pennycook, S. J.; Chisholm, M. F. *Small* **2012**, *8*, 3283−3288.
(48) Byun, J.; Je, S.-H.; Patel, H. A.; Coskun, A.; Yavuz, C. T. *J. Mater. Chem. A* **2014**, *2*, 12507−12512.
(49) Zhu, X.; Chi-Linh, D.-T.; Murdock, C. R.; Nelson, K. M.; Tian, C.; Brown, S.; Mahurin, S. M.; Jenkins, D. M.; Hu, J.; Zhao, B.; Liu, H.; Dai, S. *ACS Macro Lett.* **2013**, *2*, 660−663.
(50) Vogiatzis, K. D.; Mavrandonakis, A.; Klopper, W.; Froudakis, G. E. *ChemPhysChem* **2009**, *10*, 374−383.
(51) Pan, H. H.; Ritter, J. A.; Balbuena, P. B. *Langmuir* **1998**, *14*, 6323−6327.
(52) Jiao, Y.; Zheng, Y.; Smith, S. C.; Du, A.; Zhu, Z. *ChemSusChem* **2014**, *7*, 435−441.
(53) Myers, A. L.; Prausnitz, J. M. *AIChE J.* **1965**, *11*, 121−127.
(54) Ren, S.; Bojdys, M. J.; Dawson, R.; Laybourn, A.; Khimyak, Y. Z.; Adams, D. J.; Cooper, A. I. *Adv. Mater.* **2012**, *24*, 2357−2361.
(55) Liebl, M. R.; Senker, J. *Chem. Mater.* **2013**, *25*, 970−980.
(56) Patel, H. A.; Ko, D.; Yavuz, C. T. *Chem. Mater.* **2014**, *26*, 6729−6733.
(57) Rabbani, M. G.; El-Kaderi, H. M. *Chem. Mater.* **2012**, *24*, 1511−1517.
(58) Zhu, Y.; Long, H.; Zhang, W. *Chem. Mater.* **2013**, *25*, 1630−1635.
(59) Zhao, Y.; Yao, K. X.; Teng, B.; Zhang, T.; Han, Y. *Energy Environ. Sci.* **2013**, *6*, 3684−3692.
(60) Xiang, Z.; Zhou, X.; Zhou, C.; Zhong, S.; He, X.; Qin, C.; Cao, D. *J. Mater. Chem.* **2012**, *22*, 22663−22669.
(61) Hug, S.; Mesch, M. B.; Oh, H.; Popp, N.; Hirscher, M.; Senker, J.; Lotsch, B. V. *J. Mater. Chem. A* **2014**, *2*, 5928−5936.
(62) Errahali, M.; Gatti, G.; Tei, L.; Paul, G.; Rolla, G. A.; Canti, L.; Fraccarollo, A.; Cossi, M.; Comotti, A.; Sozzani, P.; Marchese, L. *J. Phys. Chem. C* **2014**, *118*, 28699−28710.
(63) Shen, C.; Wang, Z. *J. Phys. Chem. C* **2014**, *118*, 17585−17593.
(64) Sekizkardes, A. K.; Altarawneh, S.; Kahveci, Z.; Islamoglu, T.; El-Kaderi, H. M. *Macromolecules* **2014**, *47*, 8328−8334.
(65) Ren, S.; Dawson, R.; Laybourn, A.; Jiang, J.-x.; Khimyak, Y.; Adams, D. J.; Cooper, A. I. *Polym. Chem.* **2012**, *3*, 928−934.
(66) Song, W.-C.; Xu, X.-K.; Chen, Q.; Zhuang, Z.-Z.; Bu, X.-H. *Polym. Chem.* **2013**, *4*, 4690−4696.
(67) Xiong, S.; Fu, X.; Xiang, L.; Yu, G.; Guan, J.; Wang, Z.; Du, Y.; Xiong, X.; Pan, C. *Polym. Chem.* **2014**, *5*, 3424−3431.
(68) Chowdhury, P.; Bikkina, C.; Gumma, S. *J. Phys. Chem. C* **2009**, *113*, 6616−6621.
(69) Presser, V.; McDonough, J.; Yeon, S.-H.; Gogotsi, Y. *Energy Environ. Sci.* **2011**, *4*, 3059−3066.
(70) Lippens, B. C.; Boer, J. H. D. *J. Catal.* **1965**, *4*, 319−323.

DOI: 10.1021/jacs.5b03579
J. Am. Chem. Soc. 2015, 137, 7210−7216